Transactions on Additive Manufacturing Meets Medicine
Trans. AMMM, Vol. 4, No 1, Article ID 701, 9 Pages

Infinite Science Publishing

Original Research Article

3D patterning – an extended toolbox for Micro-Electro-Mechanical Systems

H. K. Trieu[1*], L. Rennpferdt[1], and S. Bohne[1]

[1] *Institute of Microsystems Technology, Hamburg University of Technology, Hamburg, Germany*
[*] *Corresponding author, email: trieu@tuhh.de*

Abstract: 3D printing and micromachining of micro-electro-mechanical systems (MEMS) are both technologies with excellent benefits, but also with some limitations. The various 3D printing processes offer a very high degree of design freedom, customizability and efficiency in material usage. Only a few have already achieved micrometer-precise resolutions. They are also very limited in their choice of materials and thus in the type of systems, often being only passive mechanical or fluidic systems. Manufacturing processes from microsystems and semiconductor engineering provide access to a wide range of materials, both conductive and dielectric. There are myriad systems such as sensors, actuators, photonic and electronic devices with resolutions in the micrometer and sub-micrometer range and tremendous integration density. However, although MEMS components are mechanically flexible and moveable in 3D, the typical MEMS designs are based on 2D layouts resulting in planar structures with limited thicknesses. They can be extended to extruded 2.5D structures with high aspect ratios by deep etching, to 3D structures with degrees of design freedom limited to specific crystal orientations by wet chemical anisotropic etching or to even more complex geometries by bonding of structured wafers. The successful combination of 3D printing and micromachining of MEMS is demonstrated in this paper with some basic technology investigations that pave the way to an extended toolbox for MEMS with high degrees of design freedom in 3D as known from 3D printing. Extending the typical one-step manufacturing approach of 3D printing to multiple processing cycles, as is common in manufacturing of microsystems and semiconductor devices, will enable 3D patterning with more complex structures and unprecedented integration density.

I. Introduction

Microsystems, also known as MEMS (Micro-Electro-Mechanical Systems) [1], are well established and indispensable in daily life, with great potential in life sciences. MEMS have their origin in semiconductor technology, a typical subtractive planar technology for the manufacturing of microelectronic devices and integrated circuits. Enhanced by specific process modules such as surface and bulk micromachining, 3D freely moving structures have been realized. However, due to the techniques used, such as photolithography, thin film deposition and reactive ion etching, the achievable devices are limited to components with planar 2D geometry and low thickness or to extruded 2.5D structures with high aspect ratio. Grey-scale lithography has enabled the transfer of 3D patterns from a resist mask into the substrate [2]. MEMS with more complex structures such as microvalves and micropumps have been implemented by bulk micromachining combined with wafer bonding techniques [3]. 3D patterning with additive manufacturing such as photopolymerization, extrusion, powder bed fusion or direct writing [4] and subtractive 3D approaches such as selective laser-induced etching (SLE) [5] are highly versatile manufacturing techniques differing in technology, materials and precision. Other advantages besides high degree of design freedom include efficiency, customization and manufacturing speed. However, although 3D printed devices can be very complex in shape, their functionality remains limited in complexity due to creating the entire structure in one fabrication step using usually only one material. Recent trends in multi-material additive manufacturing show more complex 3D printed parts [6] with applications for printed electronics [7]. Nevertheless, the complexity of functionality and integration density of MEMS remain unmatched. Manufacturing of 3D MEMS with high degrees of design freedom, as known from additive manufacturing, in combination with complex functionalities of traditional

microsystems is still in its infancy and subject of current research.

Despite of two decades of research in combining the two technologies of 3D printing and MEMS, progress has been achieved mainly in the fields of microfluidics and packaging where devices with dimensions clearly beyond some tens to hundreds of micrometers are compatible to the fairly coarse minimum feature size of most of the 3D printing techniques. Only few 3D printing methods provide high resolution in the micrometer regime and below, as discussed in the two reviews [8, 9]. In [8] additive rapid prototyping technologies, such as stereolithography (SLA), fused deposition modeling (FDM) and selective laser sintering (SLS), are reviewed and compared with the resolution requirements of the traditional MEMS fabrication methods. This review from 2014 concludes that microfluidic and lab-on-a-chip devices for fluid handling and manipulation as well as electronic packaging appear to benefit greatly from the advances in the 3D print area with minimum feature size of 50-500 µm. Further developments in the 3D materials and printing methods are considered as inevitable for the use of 3D printing for MEMS sensors and actuators. Apart from the goal to drive toward micrometer resolution, these requirements include aspects as adhesion of 3D printed materials, wafer-level printing, gas- and vacuum-tight materials, and combination of dielectric and conductive materials creating electronic and active devices like strain gauges, capacitors, electrodes and electrostatic drives. The more recent overview of developments and applications in 3D printing of MEMS from 2020 [9] still confirms the trends for microfluidic systems and MEMS packaging respectively MEMS assembly. But also few MEMS sensors and actuators are recently realized by 3D printing, e.g. a 3D printed MEMS accelerometer [10], a thermomechanical [11] and an electrostatic actuator [12]. All three devices particularly benefit from advances in two-photon polymerization (2pp) enabling high speed 3D printing with minimum feature size below 1 µm. Using 2pp-printed T-shaped shadow-masking structures electrical interconnects and electrodes are created by directional evaporation or sputtering of metal thin films [10-12]. For more established 3D printing techniques, new ideas emerged how to reduce the minimum feature size, in this way making 3D printing more and more suitable for MEMS fabrication.

II. Methodology

Here, a hybrid approach to integrating 3D patterning techniques as an extended toolbox for wafer-level fabrication of 3D MEMS including photonic waveguides is presented. In the following, these 3D devices with high degrees of design freedom, as known from additive manufacturing, in combination with complex functionalities of traditional microsystems are briefly referred to as 3D MEMS. A schematic representation of the toolbox is depicted in Fig. 1. In order to manufacture more complex integrated 3D MEMS, individual process flows composed of specific process steps from the extended toolbox including optional repetition of steps can be created, going beyond the single-step manufacturing approaches of current 3D printing methods. Examples of the extended toolbox elements are two-photon polymerization (2pp), selective laser etching (SLE), femtosecond laser writing (FLW), laser welding, and ultra-precise deposition direct printing (UPD). Further 3D printing approaches with compatible resolution can be added in future. These well-defined process steps for 3D patterning can be integrated arbitrarily and repeatedly into the multiple processing cycles of MEMS manufacturing. For this the process steps have to be self-contained and compatible with the traditional process flows, which will be examined in more detail in this work to proof the feasibility of an extended toolbox for MEMS. The compatibility of 3D patterning and MEMS is considered in terms of their micrometer and sub-micrometer resolution and precision, respectively, as well as material compatibility and the ability to establish a tight connection between a patterned wafer and the 3D printed structures.

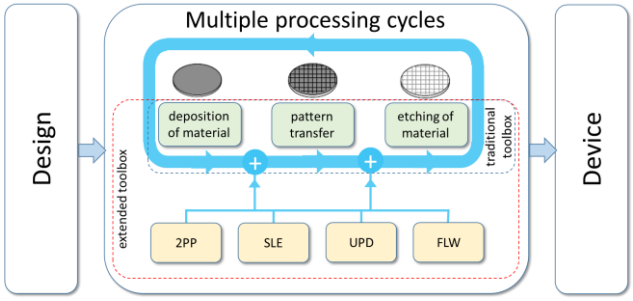

Figure 1: Concept of an extended toolbox for 3D MEMS. The common MEMS multiple processing cycles approach is denoted with a traditional toolbox made of process modules for deposition of material, pattern transfer and etching of material. The extended toolbox approach expands this process flow by optionally integrated 3D patterning process steps. SLE can be used to create 3D structures made of glass (e.g. fused silica), photonic waveguides can be integrated in a glass wafer, by laser-welding glass wafers or glass and silicon MEMS wafers can be bonded to create more complex devices, 2pp can print 3D structures on structured silicon and in or on glass wafers. With UPD direct printing of metals and dielectrics on arbitrary surfaces with 3D topography can be performed. Thin film deposition from the traditional toolbox can also be used to coat 3D structured wafers. Patterning of the thin films on the 3D topography is achieved by the femtosecond laser processing. Each process step can be repeatedly used in term of multiple processing cycles respecting material and process compatibility.

The additional process steps of the extended toolbox can be classified into methods for 3D printing at micrometer scale and methods for 3D structuring on surfaces and in-volume, respectively. Key elements of such a toolbox are processes that enable:

i) 3D printing on and/or in a MEMS device or wafer with stable contact between both giving good adhesion,

ii) on wafer level 3D printing with bonding of the 3D patterned wafer and the MEMS wafer enabling gas- and vacuum-tight interfaces,

iii) electrical contact and insulation of 3D patterned surfaces as well as electrical interconnection between the MEMS wafer and the 3D patterned structures creating contact pads, electrodes or capacitors.

iv) Furthermore, 3D patterning of photonic waveguides will enable the realization of 3D photonic microsystems, the co-integration of 3D photonics and MEMS, as well as optical interconnection.

III. Results and discussion

In this section, results of the individual process steps of the toolbox addressing the previous mentioned four key elements are presented and examined with regard to their compatibility for integration into the process flow. Two high-precision 3D patterning techniques, selective laser-induced etching and two-photon polymerization, have been applied for 3D MEMS such as a gas dynamic virtual nozzle (GDVN) [13]. In addition, an ultra-precise deposition (UPD) direct printing method for the direct writing of metals and dielectrics on 3D surfaces and femtosecond laser writing (FLW) of integrated waveguides have been investigated.

III.I. Two-photon polymerization printed GDVN on a MEMS fluidic chip

The first toolbox example is the interconnection of a micronozzle using 2pp by direct printing on a glass-silicon microfluidic chip. The micronozzle is a GDVN nozzle in which the desired liquid jet is more focused by additionally introduced helium gas so that the resulting jet is only a few micrometers wide [14]. Thus the mechanical nozzle orifice can be much larger (diameter: 30-60 µm) than the jet diameter. This has several advantages: Less manufacturing accuracy is required, the nozzle is much more reliable against clogging, and the width and length of the water jet can be regulated by adjusting the gas and liquid flow. Such nozzles are used as sample delivery systems in serial femtosecond crystallography (SFX) experiments [15]. Here, the jet from the nozzle is enriched with a protein, crystal, or virus sample to be studied and then directed toward the X-ray beam. A complete diffraction pattern is assembled from the diffraction patterns of the small samples fed one by one, from which the structure of the sample can be deduced.

2pp enables 3D patterning with a minimum resolution of about 200 nm and great design freedom [16, 17]. This allows the fabrication of novel structures and geometries in the field of microfluidics, e.g. micromixers, micronozzles and the combination of both. The very high resolution limits the maximum size of the 2pp device, so that effectively only the needed structures should be manufactured with the high 3D design freedom and resolution. Therefore, we combine the 2pp GDVN nozzle with a chip manufactured with standard MEMS technology, which enables the integration of additional functions into the chip, such as thin-film sensors or actuators. It has already been shown in publications that such a combination is useful and creates added value, e.g. 2pp microsieves, mixers, or valves in channels fabricated in silicon and glass or in PDMS [18, 19].

A 3D drawing in Fig. 2 shows the assembly of the nozzle and chip with the fluidic connection to the laboratory through fused silica capillaries. The MEMS chip is designed such that the input capillaries can all be easily glued into the chip on one side. Up to three capillary openings are prepared, with channel sizes matched the capillaries used. Only two are used for the presented GDVN, for the aqueous sample and for the focusing gas. The chip is made of two wafers, one glass and one silicon, both patterned by MEMS methods and then bonded by anodic bonding. A detailed description of the design and fabrication process is published by Bohne et al. [13].

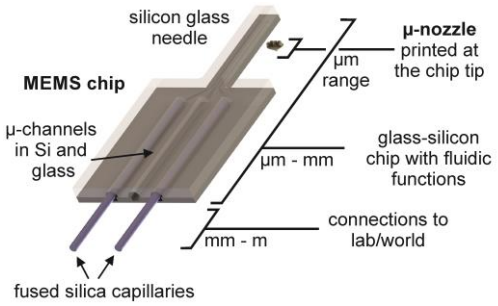

Figure 2: 3D rendering of the developed silicon glass MEMS chip with two inlet capillaries and the printed nozzle.

After the chip is fabricated, the nozzle is printed on the end opposite the capillaries. The nozzle side of the chip was formed into a needle and all excess silicon and glass was removed so as not to obstruct the X-ray beam.

The nozzle design is based on previously published work [20-22]. There, the GDVNs were fabricated without a MEMS chip, and the capillaries were directly connected to the 2pp nozzle. This means that the nozzle was extended in length by a factor of 2-3 to allow the capillary to be glued in. Direct gluing into the less than 1 mm³ small nozzle, while possible, is much more difficult and carries a greater risk of clogged capillaries than gluing onto the MEMS chip. In addition, the printing time increases significantly for the coarser gluing structures. The nozzle orifice and liquid guiding are kept similar in order to compare the performance of the nozzles.

A particular challenge in the connection of MEMS fluidic chip and nozzle is the stress on the connection due to the high internal pressure of gas and liquid. This must not be neglected, as the nozzle will naturally detach from the chip due to the pressure. It is not sufficient to simply print the 2pp structure on the silicon surface. Additional anchors were designed and printed in matching counterparts on the

silicon chip (key-lock principle). These so-called “roots” significantly improve adhesion. Additionally, gaskets were printed into the silicon ducts. These 2pp hollow cylinders fit into the silicon ports. As soon as the internal pressure increases, the flexible 2pp material is pressed against the channel wall, improving the sealing.

The GDVN design is shown in Fig. 3. For simplicity and to allow quick design changes, the nozzle was divided into three independent parts: tip, main body and root structures. The design of each can be changed very quickly and easily as long as the interface geometry remains fixed. Several nozzles with different design and process variations were written with the material IP-S 2pp-resist (Nanoscribe GmbH, Karlsruhe, Germany) using a 25x DILL (dip in laser lithography) objective on a Nanoscribe Photonic Professional GT.

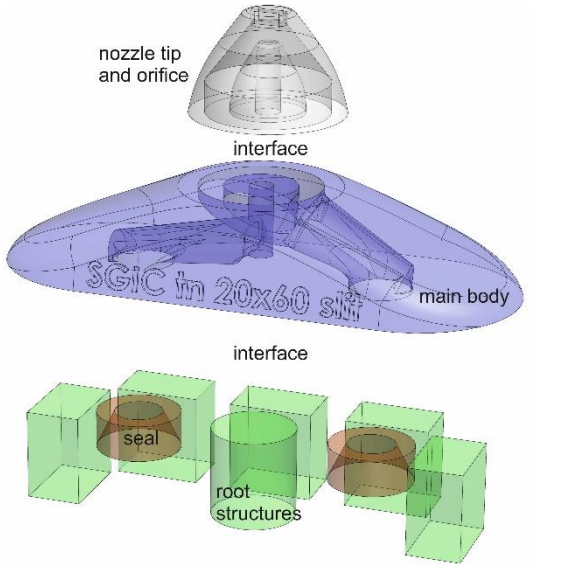

Figure. 3: Design of a 3D printed nozzle. The three independent components of the nozzle: nozzle tip and orifice, main body with fluid channels, and root and seal structures, which help to bond the printed material to the silicon.

Standard 2pp printing and direct printing on a MEMS chip differ significantly in the process details. The standard printing is done on commercially available and cleaned glass. The detachment of the 2pp objects from the glass during development of the written resist is usually desired. In our case, an extremely clean MEMS chip, cleaned with acetone, isopropanol and water, is essential for good adhesion of the nozzle on and in the chip. A series of chips were mounted in a custom fixture and aligned with the GDVN print job. In addition, we start the writing process "deeper" in the material (100 µm below the surface to realize the roots and sealing lips) and to achieve very good and strong polymerization directly on the silicon. Since silicon is more reflective than standard glasses, the laser energy has to be adjusted to avoid micro-explosions of overexposed resist that would otherwise occur.

For simplified, robust alignment, the root and seal structures are enlarged so that an alignment of 10 µm is sufficient and the "key" always fills the entire keyhole. This improves adhesion and prevent leakage. Another challenge was the development of the photoresist. The MEMS chip prevents the developer from reaching the back of the nozzle. Instead, the chemicals have to diffuse through the long channels of the chip. This greatly increases development time, but is still a very simple passive batch process. Fig. 4 shows the robust alignment and the processed nozzle on top of the MEMS chip.

After gluing the fused silica capillaries with a diameter of 360 µm, the nozzle chips could be characterized. The water or the aqueous sample was pumped into the chip using a syringe- or HPLC pump. The volume flows were between 1.5 and 700 µl/min, the helium flow regulated between 6 and 112 mg/min was provided by a pressurized gas bottle and adjustable pressure reducers (up to 5 MPa).

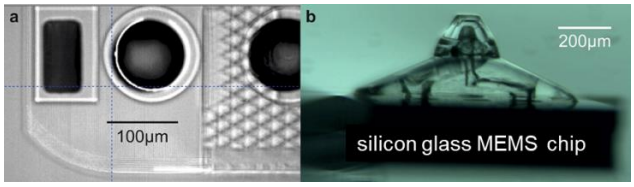

Figure 4: Micronozzle printed on chip: (a) View from above of the nozzle during the printing process. The rectangular roots and the circular sealing structures are visible. (b) An optical microscope image of a printed nozzle on the MEMS chip (side view). The nozzle is 850 µm wide, 350 µm high, and 310 µm deep.

With the smaller volume flows, very stable jets with a suitable length and diameter for SFX could be generated. The jets are visible in Fig. 5, (a) in air atmosphere and (b) in vacuum.

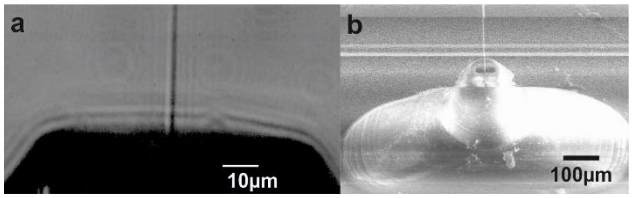

Figure 5: Nozzle jet testing: (a) An image of a liquid jet propagating into the air. The jet diameter is approx. 1.5 µm. (b) An image of a liquid jet in vacuum at 100 Pa at higher flow rates. The jet diameter is about 5 µm.

The high flow rates were used to test the adhesion of the nozzle to the chip until failure. It was shown that the root and the sealing structures had a significant influence on the maximum possible flow and thus the internal pressure [13].

In-channel 2pp structures and the printing of optical elements onto a MEMS chip without mechanical stress have already been shown in publications [18, 19, 23]. In our example, two fluidic components were connected, where the challenge of tightness, connection strength and thus reliability is in the focus. Direct printing of a 3D micro-GDVN using 2pp into and onto a glass silicon MEMS chip could be demonstrated. The performance of the nozzle is equivalent to the stand-alone 2pp printed

nozzles, but allow the integration of more functions by the used MEMS platform.

One limiting factor is the sensitivity of the 2pp material to the traditional MEMS toolbox processes. The etching solutions, plasma processes or high temperature destroy the 2pp structure, so that the 2pp process should be carried out at the end before the chips are diced out of the wafer.

III.II. 3D fused silica devices by in-volume selective laser etching

The second example from the toolbox is the fabrication of 3D microfluidic devices by in-volume SLE, also known as femtosecond laser induced chemical etching (FLICE). This technology creates inverted structures compared to 2pp. It is a subtractive process that uses femtosecond infrared lasers to treat glass in such a fashion that the exposed volume can be etched 100 to 1000 times faster than the unexposed material in potassium hydroxide (KOH). In contrast, 2pp materials are like negative photoresists, with the area exposed by the laser is fixed during development, and the unexposed rest is removed.

The laser-writing path corresponds to the inverse 3D model of the device and any 3D design can be realized as long as the exposed volume is accessible to etch attack (see Fig. 6a). The enhanced etch rate is achieved due to the principles of non-linear photoionization and ultrashort laser pulses. Only in the focal point with concentrated photons where the energy of several photons interact, the glass material is modified by formation of nanogratings resulting in an increased etchability [24]. Glass material surrounding the focus is not affected by the 1030 nm wavelength. The laser focus can be moved freely in the volume with xyz stages and a galvo scanner directs the writing of the desired volume. This method is particularly suitable for small microfluidic structures, since the mostly small channels and cavities are written, but not the complete bulk material as necessary with the 2pp method.

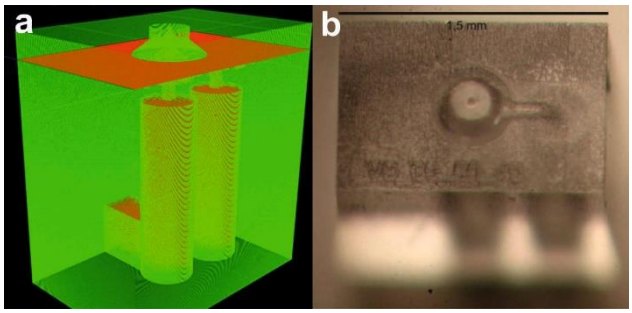

Figure 6: (a) Nozzle design and laser scribing paths: green - slice lines follow the outer contour of the chip and nozzle; red - fine hatch lines fill the cavities and areas to be etched. (b) Glass nozzle after completion, with a nozzle opening of approx. 50 µm.

Fused silica (amorphous quartz glass) is one of the most popular and best-researched glass for SLE processes. This glass allows robust processes with a high degree of design freedom. We have fabricated a similar GDVN design from chapter III.I. in fused silica glass (see Fig. 6b). With the glass micronozzles described here, stable water jets with a diameter of 2.5 µm and a length of 200 µm are generated at a sample flow of 5 µl/min and gas flow of 9 mg/min (see Fig. 7).

The SLE process (laser: 1030 nm, 765 kHz, 0.3 ps with 20x0.4 NA lens, 2 µm contour spacing, 5 µm hatching spacing) optimized at the Institute of Microsystems Technology at Hamburg University of Technology for very small structures can be used to produce complex fluidic devices with high resolution on a LightFab 3D Printer (manufacturing version). The design freedom of 3D laser processing with SLE makes it possible to produce novel geometries and small dimensions very quickly (rapid prototyping).

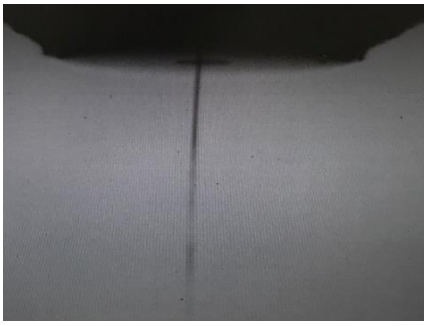

Figure 7: Glass nozzle test of the smallest possible fluid jet in air, jet diameter approx. 2.5 µm, length approx. 200 µm.

Compatibility with traditional MEMS technologies is basically already given. Fused silica wafers and many other glass wafers are commercially available in CMOS quality with regard to homogeneity and roughness. The LightFab 3D Printer (manufacturing version) can process wafers up to 200 mm in diameter. The fabrication of many systems on one wafer can be even simpler than on small single chips, as the alignment at wafer level is known from the MEMS processes. Handling during KOH etching and water rinsing is also much more convenient on wafer size than on many tiny chips.

The glass wafer or components can be bonded to the MEMS chips using various bonding technologies. Fused silica can be bonded to fused silica or other glasses by laser welding. Laser welding can be done by a process similar to SLE with adjusted parameters (laser: 1030 nm, 2067 kHz, 0.4 ps with 20x0.4 NA lens). The surface of the glass parts to be welded must be as smooth as possible to achieve a good welding result. Consequently, laser-machined surfaces cannot be welded directly, as they have an increased roughness after KOH etching. Unmachined surfaces should be positioned as close as possible. In Figure 8 (a) a microfluidic chip is shown made of one SLE structured fused silica chips bonded by laser welding to a second non-structured fused silica cover glass. In Figure 8 (b) several parallel welding seams are visible, the width of

one single seam is about 50 µm. Fused silica and silicon are also bondable by laser welding [25].

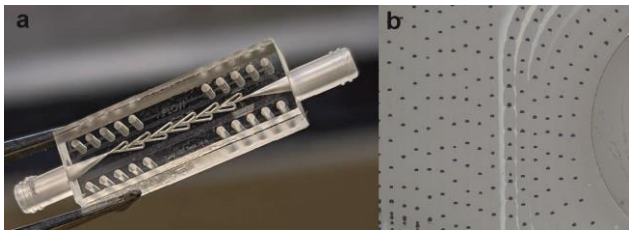

Figure 8: (a) A microfluidic chip with a Tesla valve made of one SLE structured fused silica chip bonded by laser welding to a second non-structured fused silica cover glass manufactured at the Institute of Microsystems Technology at Hamburg University of Technology. (b) Magnification of parallel welding seams with a width of one single seam of 50µm.

SLE processes with borosilicate glass chips have already been published [26, 27]. The selectivity is somewhat lower than for fused silica, but 3D devices can be manufactured. This should also make it possible to transfer the process to entire wafers. In that case, standard anodic bonding between the borosilicate glass and silicon wafer can be used. Other bonding processes with intermediate layers such as gluing and eutectic bonding are also possible.

An extension of the toolbox with SLE is therefore possible. However, there is the restriction that the SLE glass structures should be completely fabricated first, as otherwise MEMS silicon and thin-film structures can be destroyed by the long etching times in highly concentrated hot KOH solution. Conversely, there is hardly any risk of fused silica being damaged in subsequent MEMS processes. Fused silica is more stable than silicon at high temperatures and also inert to most etching solutions used. Even hydrofluoric acid baths and plasma etching are possible, as the etch rates for the MEMS nanometer thin films to be patterned are usually irrelevant for the micrometer thick fused silica structures.

III.III. Ultra-precise deposition direct printing of metals and dielectrics

A further building block of the toolbox is a direct printing method for metals and dielectrics. Using an UPD technique, lines and dots can be written on variable substrates and surfaces with a resolution in the micrometer range. The writing process has been described in detail by Łysień et al. [28].

The basic setup of this technique is shown in Fig. 9. A specially developed high viscosity paste is extruded through a micronozzle onto the substrate under precise pressure control. During this process, the viscosity of the paste decreases due to shear thinning at the nozzle tip, making it printable. As soon as the paste leaves the nozzle, it returns to its stable initial state, allowing printing on surfaces with a wide range of wetting properties. Structures with dimensions of 1-10 µm can be printed using different printing nozzles from 0.5-10 µm and correspondingly optimized pressures. By using an xyz positioning system, a precise, well-defined distance between substrate surface and printing nozzle can be kept constant, enabling printing on 3D surfaces. A subsequent sintering step of the printed structure increases the conductivity of metallic structures.

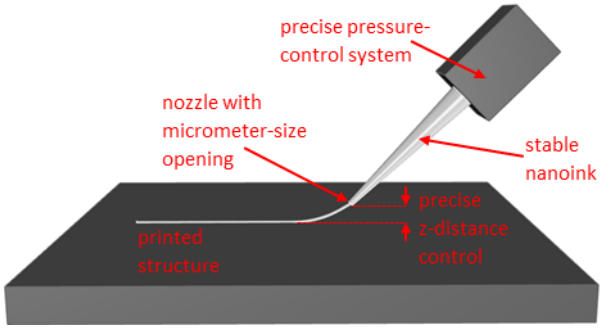

Figure 9: Principle setup of the ultra-precise deposition printing technique.

As a proof-of-principle for the integration of this additive UPD printing method into the extended toolbox for MEMS, we wrote silver electrical traces and contact pads on a 3D patterned surface of fused silica. For this purpose, trenches with a depth of 100 µm and different geometries (semi-circular, v-groove with a slope of 45°, square cross sections with slope angles of 70°, 80° and 90°) were first patterned on the substrate surface using the SLE method described previously. The surface roughness of the patterned trenches in this case is about 1 µm (rms).

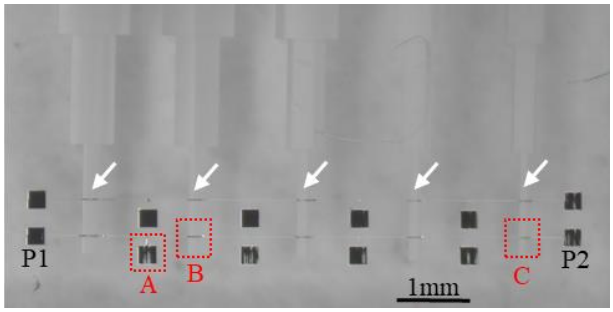

Figure 10: Top view of the printed silver structure using UPD printing on 3D patterned fused silica surface. The rectangular contact pads are clearly visible. The outer contact pads are each connected with slightly visible traces. The contact pads in the center are each connected vertically upwards to the horizontally aligned traces. The white arrows indicate the five trenches with a depth of 100 µm and different geometries. The areas marked in red are shown magnified in Fig. 11.

Delta Printing System (XTPL S.A., Poland) was used to write conductive paths across the patterned channels. The applied printing material was silver (XTPL CL85 Ag Nanopaste, XTPL S.A., Poland) and a printing nozzle with an orifice of 5 µm (XT_N50, XTPL S.A., Poland) was used. After printing, the substrate including the written structures was sintered on a hot plate at 200 °C for 20 minutes. The result can be seen in Fig. 10. with traces crossing all trenches. Contact pads were written on the unstructured substrate surface on the input and output sides and between the trenches to investigate the conductivity at

different positions. A conductive connection across all trenches was successfully established. The resistance was measured as 120 Ω/mm by a 4-point measurement between the P1 and P2 contact pads. For a closer look at the structures, an enlargement of a contact pad is shown in Fig. 11 (a).

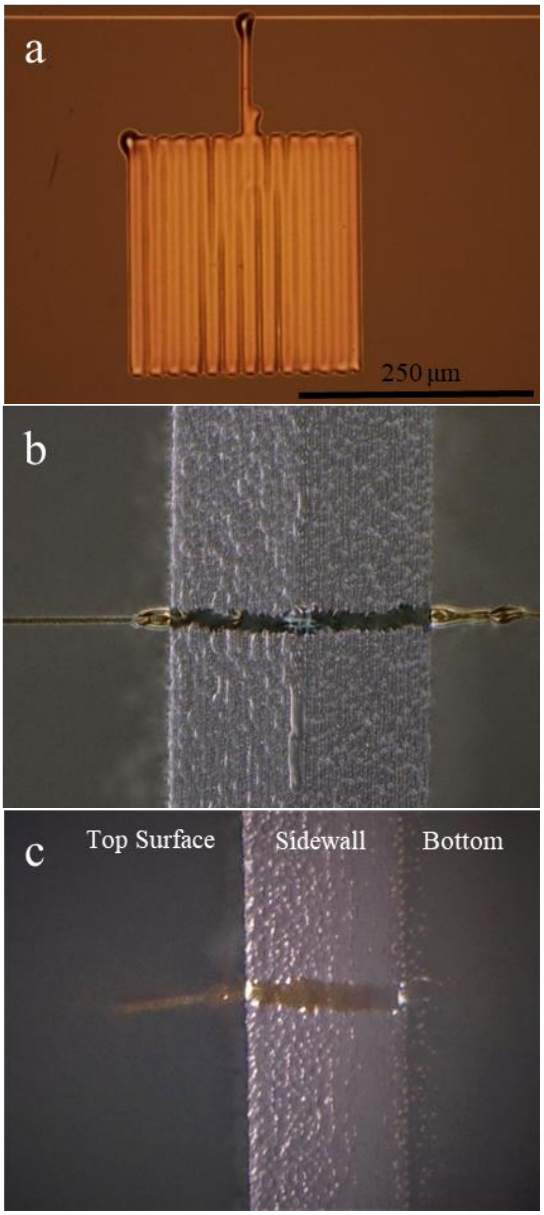

Figure 11: Magnifications of the printed silver structure shown in Fig. 10. (a) shows a contact pad. Individual manually written lines merge into a surface. Artefacts can be seen e.g. at the connection to the horizontal trace. (b) Top view of the traces passing the v-groove trench with sidewall slopes of 45°. (c) Tilted top view at 45° of the trace crossing the 90° slope sidewall of the rectangular trench with a step height of 100 µm.

Fig. 11 (b) and (c) show the magnification of the written traces within the trenches. In (b) the metal trace through the v-groove trench is shown. In the trenches, the paths were also written manually, having a width of about 13 µm on the rough, textured surface. In (c) a written path on a sidewall with 90° slope can be seen. The inclined alignment of the print nozzle enables writing on vertical sidewalls.

The presented experiment shows that UPD printing of conductive structures on 3D patterned fused silica substrates with significant surface roughness is feasible. So far, only silver is available as a conductive material in the form of nanopaste; an expanded selection of materials is expected from the manufacturer in the future. This would greatly expand the possible applications in the toolbox.

In addition, dielectrics can also be written in the same way using SU-8 (Sigma-Aldrich) as the printing material [28]. Further automation of the process during writing inside the trenches can be realized with a previously performed surface mapping. The writing of traces with a smaller width has to be further investigated regarding the given surface roughness on structured surfaces. Alternatively, the roughness of the patterned surface can be reduced by thermal treatment in an intermediate step [29]. Nevertheless, this proof-of-principle also demonstrates the relevance of this technology for 3D patterning of MEMS. In addition to electrical circuits on complex surfaces, this technology can potentially be used to realize interconnects between stacked layers.

III.IV. Femtosecond laser writing of integrated waveguides

Another 3D patterning technique related to the toolbox is the integration of 3D waveguides into the bulk substrate using femtosecond lasers, so called femtosecond laser writing (FLW). This direct writing technique offers the possibility of increasing the complexity of MEMS structures. Typically, integrated optical waveguide fabrication is limited to 2D or 2.5D by patterning a previously deposited thin film on the surface using a lithography process. Femtosecond lasers offer the possibility of integrating 3D waveguides into the substrate by locally modifying the bulk material. In contrast to previously mentioned SLE process, the non-linear FLW process is performed at lower energy input to avoid nanogratings and obtain local refractive index increase (type I modification) in the focal volume due to material densification [30]. A higher energy input, on the other hand, generates damaged written tracks with densification of the material in the surrounding areas resulting in a decrease of the refractive index (type II modification) [31]. By directing the focus through a transparent substrate the waveguide core, respectively the waveguide cladding, can be written, leading to a variety of different possibilities for 3D integrated waveguides [30-32].

For our concept of an extended toolbox for MEMS, these flexibly fabricated waveguides offer themselves as an enhancement option for more complex systems. In first experiments, waveguides with type I modification were written in a fused silica substrate and investigated. The propagation losses and polarization dependence of the

waveguide as a function of different laser parameters were investigated. Waveguides with a length of 3 mm were written with laser wavelength of 1030 nm and 515 nm at circular polarization. The laser was focused 100 µm below the surface. After writing, the waveguides were cut at the end facets with a dicing machine and examined at a wavelength of 1550 nm. Light was coupled into the waveguides using a lensed single mode fiber and captured at the output with a lens, collimated into a fiber, and directed to a detector.

Fig. 12 shows an example of the top view and cross section of fabricated waveguides with a writing laser wavelength of 1030 nm, a repetition rate of 504 kHz, a laser pulse duration of 300 fs, a pulse energy of 100 nJ, a writing speed of 50 mm/s, and a varying repetition of the write path from 1 to 3. The top view (a) shows smooth waveguides. The cross section (b) shows the elongated shapes of the laser-modified regions. The brighter region visible here has an increased refractive index and thus acts as a waveguide core as reported in the literature [33].

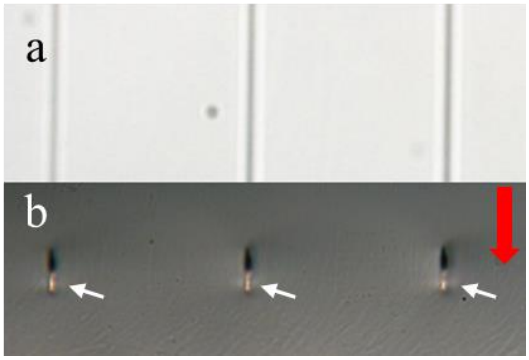

Figure 12: Top view (a) and cross-sectional view (b) of FLW waveguides of type I. The distance between each waveguide is 100 µm. Three waveguide paths were written with multiple repetition of the writing path from 1 (left waveguide) to 3 (right waveguide). The top view shows smooth waveguides. The modified regions of the bulk substrate are clearly visible. The bright areas shown by the white arrows indicate the light-guiding waveguide cores. The red arrow indicates the direction of the femtosecond laser. The cross-section was manually polished.

Fig. 13 shows the lowest propagation losses achieved to date for a laser wavelength of 515 nm, repetition rate of 1008 kHz, pulse duration of 300 fs, pulse energy of 250 nJ and writing speed of 50 mm/s. Propagation losses of 0.518 dB/cm were obtained. The high coupling losses are likely due to non-polished end facets and reflections. In addition, the polarization dependence of waveguide length was determined with cutback method and a coupled polarization filter. It was found that the polarization does not change over the length of the waveguide.

Moreover, this method of FLW 3D waveguides allows the insertion of sensors [34] and is not limited only to glass but is also suitable for polymers transparent to the laser wavelength [35]. However, the obtained refractive index difference does not allow radii of curvature in the order of a few millimeters or even micrometers, making integration into tiny MEMS components difficult.

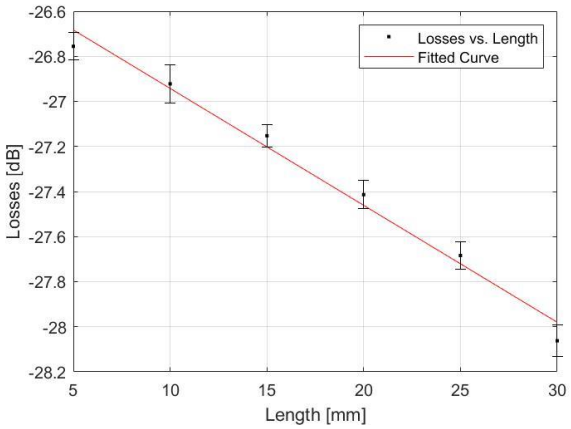

Figure 13: Cutback measurement of a FLW waveguide sample. The losses are shown as a function of the waveguide length. The slope of the fitted curve corresponds to the propagation losses with 0.518 +/- 0.069 dB/cm.

IV. Conclusions

Some successful combinations and integration of 3D printing and MEMS technology have been shown in the previous chapters. These are initial examples which demonstrate the feasibility of the concept of an extended toolbox for 3D MEMS.

As indicated schematically in Figure 1, these well-defined process steps of the extended toolbox can be successfully integrated into the process flow of the traditional toolbox, although some limitations must be considered. With respect to the key elements of an extended toolbox defined in section II, additive 3D printing on MEMS devices with sufficiently good interconnect could be successfully demonstrated as well as subtractive complex 3D patterning and bonding of typical MEMS wafers. Furthermore, high-precision patterning of conductive layers on 3D printed surfaces as well as 3D in-volume modification of optical waveguides in structurable substrates could be realized. All demonstrated methods are also consistent in precision with structure sizes of MEMS devices. The compatibility of these individual process steps with each other as well as with traditional MEMS processes was demonstrated with only a few limitations. This allows for more complex designs due to more individual and diverse combinations of the steps in the process flow. The defined process steps can be integrated into the process chains without extensive adjustments, whereby the process development can be modularized with this toolbox.

In summary, despite some limitations, with the extended toolbox presented, 3D printing and 3D surface as well as in-volume structuring can be embedded into a concept with multiple processing cycles, as is common in microsystems and semiconductor engineering. Using this approach, considerably more complex process flows can be

simplified and previously unfeasible MEMS structures can be realized. The feasibility of novel 3D MEMS devices is enabled by the added-value of 3D patterning previously not available for MEMS manufacturing and by adopting the multiple processing cycles of traditional micromachining to the normally single-step manufacturing approach of 3D printing. 3D structures can be further functionalized with coatings which can be patterned to produce complex sensors and actuators. The design freedom known from conventional 3D printing processes can be combined with the precision, resolution and material diversity of traditional MEMS processes. Comparing to the traditional planar MEMS devices, with the high resolution in the micrometer range of 3D printing, 3D MEMS will enhance the integration density of MEMS functionality by exploiting the third spatial dimension for integration.

Future advances in 3D printing in terms of miniaturization, manufacturing speed, and material mix will further enhance the toolbox. The two worlds of MEMS and 3D printing will continuously converge and produce promising solutions. Devices that were previously unfeasible or required a significantly complicated process or machine effort are now possible through innovative use and combination of the toolbox solutions presented here.

ACKNOWLEDGMENTS

The BMBF funding for ForLab (*Forschungslabor Mikroelektronik Deutschland*) HELIOS for the co-integration of photonics and electronics, which supplies the femtosecond laser equipment for 3D patterning, is highly acknowledged. The authors would also like to thank XTPL for performing the UPD printing on our 3D patterned glass substrates. Our long-term collaboration with Henry Chapman and Saša Bajt developing and testing the GDVN is highly appreciated. Last but not least we would like to thank our students Jaisinh Bhosale and Sibasish Laha for processing the GDVN and Tesla valve in SLE and Aathira Harilal for processing the FLW waveguides.

AUTHOR'S STATEMENT

Author states no conflict of interest. Informed consent has been obtained from all individuals included in this study.

REFERENCES

[1] M. K. Mishra et al., MEMS Technology: A Review, JERR, 4(1): 1-24, Article no. JERR.46001, 2019.
[2] C. M. Waits et al., Microfabrication of 3D silicon MEMS structures using gray-scale lithography and deep reactive ion etching, Sensors and Actuators A: Physical, vol. 119, no. 1, pp. 245-253, 2005.
[3] A. Bußmann et al., Piezoelectric Silicon Micropump for Drug Delivery Applications, Appl. Sci., 11, 8008, 2021.
[4] S. K. Parupelli et al., A Comprehensive Review of Additive Manufacturing (3D Printing): Processes, Applications and Future Potential, American Journal of Applied Sciences, 16 (8), pp. 244-272, 2019.
[5] J. Gottmann et al., Selective Laser-Induced Etching of 3D Precision Quartz Glass Components for Microfluidic Applications - Up-Scaling of Complexity and Speed, Micromachines 8(4), 110, 2017.
[6] S. Hasanov et al., Review on Additive Manufacturing of Multi-Material Parts: Progress and Challenges, J. Manuf. Mater. Process., 6(1), 4, 2022.
[7] G. L. Goh et al., 3D printing of Multilayered and Multimaterial Electronics: A Review, Adv. Electron. Mater., 7, 2100445, 2021.
[8] V. A. Lifton et al., Options for additive rapid prototyping methods (3D printing) in MEMS technology, Rapid Prototyping Journal, 20/5, pp. 403–412, 2014.
[9] T. Blachowicz et al., 3D Printed MEMS Technology - Recent Developments and Applications, Micromachines, 11, 434, 2020.
[10] S. Pagliano et al., Micro 3D printing of a functional MEMS Accelerometer, Microsystems & Nanoengineering, 8:105, 2022.
[11] S. Kim et al., A Two-Step Fabrication Method for 3D Printed Microactuators: Characterization and Actuated Mechanisms, Journal of Microelectromechanical Systems, vol. 29, no. 4, 2020.
[12] S. Kim et al., Fabrication and characterization of 3D printed out-of-plane torsional comb-drive actuators for microrobotics, 21st International Conference on Solid-State Sensors, Actuators and Microsystems (Transducers), 2021.
[13] S. Bohne et al., 3D printed nozzles on a silicon fluidic chip, Review of Scientific Instruments 90, 035108, 2019.
[14] M. Gañán-Calvo et al., Generation of steady liquid microthreads and micron-sized monodisperse sprays in gas streams, Phys. Rev. Lett. 80, 285, 1998.
[15] H. N. Chapman et al., Femtosecond X-ray protein nanocrystallography, Nature 470, pp. 73-77, 2011.
[16] X. Wen et al., 3D-printed silica with nanoscale resolution, Nature Materials, pp. 1506–1511, 2021.
[17] V. F. Paz et al., Development of functional sub-100 nm structures with 3D two photon polymerization technique and optical methods for characterization, J. Laser Appl. 24, 042004, 2012.
[18] L. Amato et al., Integrated three-dimensional filter separates nanoscale from microscale elements in a microfluidic chip, Lab Chip 12, pp. 1135-1142, 2012.
[19] M. H. Olsen et. al, In-chip fabrication of free-form 3D constructs for directed cell migration analysis, Lab Chip 13, pp. 4800-4809, 2013.
[20] G. Nelson et al., Three-dimensional-printed gas dynamic virtual nozzles for x-ray laser sample deliver, Opt. Exp. 24, pp. 11515-11530, 2016.
[21] M. Wiedorn et al., Rapid sample delivery for megahertz serial crystallography at X-ray FELs, Nature Communications 9, 4025, 2018.
[22] J. Knoska et al., Ultracompact 3D microfluidics for time-resolved structural biology, Nature Communication 11, 657, 2020.
[23] S. Thiele et al., Ultra-compact on-chip LED collimation optics by 3D femtosecond direct laser writing, Optics Letters Vol. 41, p. 3029, 2016.
[24] C. Hnatovsky et. al., Fabrication of microchannels in glass using focused femtosecond laser radiation and selective chemical etching, Appl. Phys. 84, pp. 47–61, 2006.
[25] I. Miyamoto et al., High speed, high strength microwelding of Si/glass using ps-laser pulses, Opt Express. Feb 9, pp. 3427-39, 2015.
[26] D. Bischof et al., Laser-assisted etching of borosilicate glass in potassium hydroxide, Optical Materials Express Vol. 11, Issue 4, pp. 1185-1195, 2021.
[27] S. Mastuo et al., Femtosecond laser-assisted etching of Pyrex glass with aqueous solution of KOH, Applied Surface Science, 255, pp. 9758-9760, 2009.
[28] M. Łysień et al., High-resolution deposition of conductive and insulating materials at micrometer scale on complex substrates, Scientific Reports 12.1, pp. 1-18, 2022.
[29] F. Sala et al., Effects of thermal annealing on femtosecond laser micromachined glass surfaces, Micromachines 12.2, pp. 180, 2021.
[30] D. Tan et al., Femtosecond laser writing low-loss waveguides in silica glass: highly symmetrical mode field and mechanism of refractive index change, Optical Materials Express 11.3, pp. 848-857, 2021.
[31] J. Burghoff et al., Origins of waveguiding in femtosecond laser-structured LiNbO3, Applied Physics A 89.1, pp. 127-132, 2007.
[32] H. Liu et al., Femtosecond laser inscribed cladding waveguides in Nd: YAG ceramics: Fabrication, fluorescence imaging and laser performance, Optics express 20.17, pp. 18620-18629, 2012.
[33] J. Guan et al., Hybrid laser written waveguides in fused silica for low loss and polarization independence, Optics express 25.5, pp. 4845-4859, 2017.
[34] A. Abou Khalil et al., Femtosecond laser writing of near-surface waveguides for refractive-index sensing, Optics Express 27.22, pp. 31130-31143, 2019.
[35] W. M. Pätzold et al., Low-loss curved waveguides in polymers written with a femtosecond laser, Optics express 25.1, pp. 263-270, 2017.